Global Change Biology WILEY

RESEARCH ARTICLE

Vegetation clumping modulates global photosynthesis through adjusting canopy light environment

Fa Li[1] | Dalei Hao[2] | Qing Zhu[3] | Kunxiaojia Yuan[3] | Renato K. Braghiere[4,5] | Liming He[6] | Xiangzhong Luo[7] | Shanshan Wei[8] | William J. Riley[3] | Yelu Zeng[1] | Min Chen[1]

[1]Department of Forest and Wildlife Ecology, University of Wisconsin-Madison, Madison, Wisconsin, USA

[2]Atmospheric Sciences and Global Change Division, Pacific Northwest National Laboratory, Richland, Washington, USA

[3]Climate and Ecosystem Sciences Division, Climate Sciences Department, Lawrence Berkeley National Laboratory, Berkeley, California, USA

[4]Division of Geological and Planetary Sciences, California Institute of Technology, Pasadena, California, USA

[5]Jet Propulsion Laboratory, California Institute of Technology, Pasadena, California, USA

[6]Canada Centre for Mapping and Earth Observation, Natural Resources Canada, Ottawa, Ontario, Canada

[7]Department of Geography, National University of Singapore, Singapore, Singapore

[8]Centre for Remote Imaging, Sensing and Processing, National University of Singapore, Singapore, Singapore

Correspondence
Fa Li and Min Chen, Department of Forest and Wildlife Ecology, University of Wisconsin-Madison, Madison, WI, USA.
Email: fli235@wisc.edu and mchen392@wisc.edu

Abstract

The spatial dispersion of photoelements within a vegetation canopy, quantified by the clumping index (CI), directly regulates the within-canopy light environment and photosynthesis rate, but is not commonly implemented in terrestrial biosphere models to estimate the ecosystem carbon cycle. A few global CI products have been developed recently with remote sensing measurements, making it possible to examine the global impacts of CI. This study deployed CI in the radiative transfer scheme of the Community Land Model version 5 (CLM5) and used the revised CLM5 to quantitatively evaluate the extent to which CI can affect canopy absorbed radiation and gross primary production (GPP), and for the first time, considering the uncertainty and seasonal variation of CI with multiple remote sensing products. Compared to the results without considering the CI impact, the revised CLM5 estimated that sunlit canopy absorbed up to 9%–15% and 23%–34% less direct and diffuse radiation, respectively, while shaded canopy absorbed 3%–18% more diffuse radiation across different biome types. The CI impacts on canopy light conditions included changes in canopy light absorption, and sunlit–shaded leaf area fraction related to nitrogen distribution and thus the maximum rate of Rubisco carboxylase activity (V_{cmax}), which together decreased photosynthesis in sunlit canopy by 5.9–7.2 PgC year^{-1} while enhanced photosynthesis by 6.9–8.2 PgC year^{-1} in shaded canopy. With higher light use efficiency of shaded leaves, shaded canopy increased photosynthesis compensated and exceeded the lost

Fa Li and Dalei Hao contributed equally and should be considered joint first author.

photosynthesis in sunlit canopy, resulting in $1.0 \pm 0.12\,PgC\,year^{-1}$ net increase in GPP. The uncertainty of GPP due to the different input CI datasets was much larger than that caused by CI seasonal variations, and was up to 50% of the magnitude of GPP interannual variations in the tropical regions. This study highlights the necessity of considering the impacts of CI and its uncertainty in terrestrial biosphere models.

KEYWORDS
canopy structure, clumping index, gross primary production, radiative transfer, terrestrial biosphere modeling

1 | INTRODUCTION

The terrestrial biosphere sequesters about 25%–30% of human-emitted carbon dioxide (CO_2; Le Quéré et al., 2018; Schlund et al., 2020). The gross terrestrial ecosystem carbon uptake by photosynthesis, gross primary production (GPP), is the largest component of terrestrial fluxes in the global carbon cycle (Braghiere et al., 2019; Jian et al., 2022; Schlund et al., 2020). Compared to data-driven models (Jung et al., 2009, 2011; Running et al., 2004; Zhang et al., 2014; Zhao et al., 2006), process-based terrestrial biosphere models (TBMs) have been playing a critical role in the coupled Earth System Models (ESMs) to prognostically estimate global carbon dynamics and future climate (Clark et al., 2011; Krinner et al., 2005; Lawrence et al., 2019; Piao et al., 2009). However, GPP remains a dominant uncertainty source in the current terrestrial carbon budget with a wide range from 112 to $175\,PgC\,year^{-1}$ (Anav et al., 2015; Baldocchi et al., 2016; Piao et al., 2013). Understanding and reducing uncertainties in GPP estimates is imperative to increase our confidence in historical simulations and future projections (Bodman et al., 2013; Collins et al., 2013; Schlund et al., 2020).

In TBMs, the upscaling of GPP from leaf to canopy scale has been demonstrated to be a major source of uncertainty. For example, with the same input datasets, Alton et al. (2007) showed globally and regionally, up to 10% and 25% of the differences in estimated GPP when using a big-leaf model versus a sunlit–shaded leaf model, respectively. Given the conceptual limitation and practical biases of the big-leaf assumption (Chen et al., 1999; Luo et al., 2018), the sunlit–shaded leaf stratification and shortwave direct-diffuse irradiance differentiation have been developed (Chen et al., 1999; De Pury & Farquhar, 1997; Luo et al., 2018; Norman, 1993; Wang & Leuning, 1998) and adopted in many regional or global TBMs (Bonan, 2019; Bonan et al., 2021; J. M. Chen et al., 2012; Chen & Zhuang, 2014; Loew et al., 2014). Sunlit leaves absorb both direct and diffuse solar radiation, while shaded leaves only receive diffuse radiation. Evidence from models and observations has shown that shaded leaves tend to have a relatively higher light use efficiency (LUE) under diffuse radiation conditions compared to that of sunlit leaves (Chen & Zhuang, 2014; Gu et al., 1999; Knohl & Baldocchi, 2008; Mercado et al., 2009; Still et al., 2009; Wang, Wu, et al., 2018; Williams et al., 2016; Yan et al., 2019). Therefore, even with the same incoming solar radiation

at the top of the canopy, differences in the partitioning of direct and diffuse radiation, and subsequently the separation of sunlit and shaded leaves within the canopy, can significantly affect canopy photosynthesis estimation (Bonan et al., 2021; Braghiere et al., 2019; Braghiere, Quaife, et al., 2020; Braghiere, Yamasoe, et al., 2020; J. M. Chen et al., 2012; Durand et al., 2021).

The randomness of the vegetation spatial distribution, quantified by the clumping index (CI), affects canopy radiative transfer processes, and thus the absorption of solar energy and photosynthesis. Leaves are generally clumped into different sub-canopy structures instead of being randomly distributed in the real world. With the same leaf area, fewer leaves are sunlit, while more leaves are shaded when the leaves in the canopy are more clumped (J. M. Chen et al., 2012). The nonrandom spatial distribution of leaves modulates canopy intercepted direct and diffuse radiation and sunlit and shaded leaf partitioning in the canopy (Bonan, 2019), with expected changes in estimated land surface energy–carbon–water fluxes (Bonan, 2019; Braghiere et al., 2019; Braghiere, Quaife, et al., 2020; J. M. Chen et al., 2012; B. Chen et al., 2016, 2021; Fang, 2021).

While ignoring CI can potentially bias estimated carbon fluxes, many TBMs (Table S1) have not yet included CI in their canopy radiation transfer schemes. Previous studies showed that ignoring CI can cause 12% less canopy photosynthesis at a temperate rainforest site (Walcroft et al., 2005) and 50% less annual net ecosystem carbon sink (Baldocchi & Wilson, 2001) at a temperate broadleaved forest site. However, at the global scale, the impacts of CI on GPP are still under debate. For example, Ryu et al. (2011) reported that CI reduced GPP by $1.5\,PgC\,year^{-1}$ in the Breathing Earth System Simulator (BESS), and Chen et al. (2012) showed $15.88\,PgC\,year^{-1}$ (~12%) less estimated annual GPP when including CI in the Boreal Ecosystem Productivity Simulator (BEPS). In contrast, Braghiere et al. (2019) showed a net increase (~$5.53\,PgC\,year^{-1}$) in estimated GPP with the Joint UK Land Environment Simulator (JULES). Albeit the important role of CI on radiative transfer, the land modules (Table S1) in many ESMs that participated in the latest Coupled Model Intercomparison Project (CMIP6; Eyring et al., 2016), such as CLM5 (Bonan, 2019), ELM (Golaz et al., 2019), LPJ-GUESS (Martín Belda et al., 2022; Smith et al., 2001), and ORCHIDEE (Krinner et al., 2005), still assumed that leaves are randomly arranged without considering CI effects (Bonan, 2019; Braghiere et al., 2019; Loew et al., 2014).

Furthermore, the majority of recent studies derived CI from the Moderate Resolution Imaging Spectroradiometer (MODIS) measurements at 500 m spatial resolution (Braghiere et al., 2019; Fang, 2021; He et al., 2012; Jiao et al., 2018; Wei et al., 2019). However, large uncertainties can be induced by different CI products with different sets of bidirectional reflectance distribution function (BRDF) models and solar zenith angle (SZA) configurations in their algorithms (Wei & Fang, 2016). The across-data CI differences and their influences on GPP estimates remain unclear. Meanwhile, considerable seasonal variations of CI have been revealed in multiple studies (Fang, 2021; He et al., 2016; Jiao et al., 2018; Ryu et al., 2010; Wei et al., 2019), while the extent to which CI seasonal variations could affect global GPP remains underexplored.

Here we explored how CI affects radiative transfer, the sunlit/shaded canopy absorbed direct/diffuse radiation, and photosynthesis at the global scale with consideration of uncertainties from multiple CI products and CI seasonal variations. We (1) included the CI effects in the radiative transfer scheme of CLM5; (2) intercompared three mostly used and publicly available spatially resolved global CI products; and (3) evaluated the impact of CI on canopy absorbed direct/diffuse radiation, and sunlit/shaded canopy photosynthesis estimates.

2 | METHODS AND DATASETS

2.1 | Model description and improvements

CLM5 is the land surface scheme of the Community Earth System Model version 2 (CESM2), which has been widely used to dynamically simulate land surface energy, hydrologic, and biogeochemical cycles (Lawrence et al., 2019). The canopy radiative transfer processes within CLM5 are represented using the two-stream approximation of Dickinson (1983) and Sellers (1985) as described by Bonan (1996) without considering the CI effects. When vegetation is clumped, vertical overlapping of leaves increases the radiation transmission probability across the canopy (Chen et al., 2012). Radiation transmission follows the Beer–Bouguer–Lambert law but with its leaf area index (LAI) multiplied by a CI Ω (Chen & Black, 1992; Nilson, 1971), as shown in Equation (1).

$$\tau = e^{-K\Omega L} \tag{1}$$

where τ is the transmittance; $K = G(\mu)/\mu$ is the optical depth of direct beam per unit area; μ is the cosine of the zenith angle of the incident beam; $G(\mu)$ is the relative projected leaf area in the direction $\cos^{-1}(\mu)$ (Ross, 1981); L is the true LAI; and Ω is the CI. When $\Omega = 1$, vegetation elements are randomly distributed, while leaves are clumped when $\Omega < 1$ and a lower value represents more clumped leaves (J. Chen et al., 2005; J. M. Chen et al., 2012; Chen & Black, 1992; Pisek et al., 2011).

The sunlit fraction of leaf area (L_{sun}) varies with the cumulative LAI x (Equation 2), and the total sunlit leaf area is its integration across the whole canopy described as Equation (3). The shaded leaf area (L_{sh}) is the difference between the total leaf area and sunlit leaf area (Equation 4).

$$f_{sun}(x) = \Omega e^{-K\Omega x} \tag{2}$$

$$L_{sun} = \int_0^L f_{sun}(x)dx = \frac{1 - e^{-K\Omega L}}{K} \tag{3}$$

$$L_{sh} = L - L_{sun} \tag{4}$$

CI alters transmittance, and further changes the upward and downward diffuse radiation scattered by leaves. According to Bonan (2019), the core two-stream approximation equations (Dickinson, 1983; Sellers, 1985) in CLM5 become Equations (5) and (6) after accounting for CI.

$$\frac{dI^\uparrow}{dx} = \left[1 - (1 - \beta)\omega\right]K_d\Omega I^\uparrow - \beta\omega K_d\Omega I^\downarrow - \beta_0\omega K\Omega e^{-K\Omega x} \tag{5}$$

$$\frac{dI^\downarrow}{dx} = -\left[1 - (1 - \beta)\omega\right]K_d\Omega I^\downarrow + \beta\omega K_d\Omega I^\uparrow + \left(1 - \beta_0\right)\omega K\Omega e^{-K\Omega x} \tag{6}$$

where $I^\uparrow$ and $I^\downarrow$, respectively, are the upward and downward diffuse radiative fluxes per unit incident flux on top of the canopy; K_d is the diffuse optical depth per unit area; ω is a scattering coefficient given by the sum of leaf reflectance and transmittance; β and β_0, respectively, are the fraction of diffuse and direct radiation scattered in the backward direction.

The optical parameters, including $G(\mu)$, ω, β, β_0, and K_d, were calculated based on the work in Bonan (1996) and Sellers (1985). Given the direct beam and diffuse albedo of the ground, the fraction of absorbed photosynthetically active radiation (FAPAR), and absorbed direct beam and diffuse radiation in sunlit and shaded canopy can be calculated respectively with the canopy structure and leaf optical parameters. Details of the calculation are described in Bonan (2019). The maximum carboxylation rate at 25°C (V_{cmax}) of sunlit and shaded canopies as a whole was the integral of leaf nitrogen content-based V_{cmax} over sunlit and shaded leaf areas in CLM5, respectively (Bonan, 2019; Luo et al., 2019). Specifically, the leaf nitrogen content $N(x)$ decreased exponentially with the cumulative LAI x from the top canopy (Equation 7). V_{cmax} was modeled to vary linearly with leaf nitrogen content $N(x)$ (Equation 8), and the sunlit and shaded canopy V_{cmax} was the integral of $V_{cmax}(x)$ and the sunlit and shaded leaf area fraction (Bonan, 2019; Chen et al., 2012; Ryu et al., 2011), described as Equations (9) and (10), respectively.

$$N(x) = e^{-K_n x} \tag{7}$$

$$V_{cmax}(x) = V_{cmax0}N(x) \tag{8}$$

$$V_{cmax,sun} = \frac{V_{cmax0}\int_0^L N(x)f_{sun}(x)dx}{\int_0^L f_{sun}(x)dx} = \frac{V_{cmax0}K\Omega\left(1 - e^{-(K_n + K\Omega)L}\right)}{(K_n + K\Omega)(1 - e^{-K\Omega L})} \tag{9}$$

$$V_{cmax,sha} = \frac{V_{cmax0} \int_0^L N(x)(1-f_{sun}(x))dx}{\int_0^L (1-f_{sun}(x))dx}$$

$$= \frac{V_{cmax0}\left(\frac{1}{K_n}\left(1-e^{-K_nL}\right) - \frac{\Omega}{K_n+K\Omega}\left(1-e^{-(K_n+K\Omega)L}\right)\right)}{L - \frac{1}{K\Omega}\left(1-e^{-K\Omega L}\right)} \quad (10)$$

where K_n is the nitrogen extinction coefficient; V_{cmax0} is the at the top-of-canopy V_{cmax}.

Introducing CI directly changes absorbed direct and diffuse radiation in sunlit and shaded leaves, and further the photosynthesis rates (Durand et al., 2021; Medlyn et al., 2011). Along with altered sunlit and shaded leaf areas (Equations 3 and 4), the canopy-level photosynthesis (A_{canopy}) was expected to be changed as well in the two-leaf photosynthesis model (Wang & Leuning, 1998) described as Equation (11).

$$A_{canopy} = A_{sun} \times L_{sun} + A_{sh} \times L_{sh} \quad (11)$$

where A_{sun} and A_{sh} are the sunlit and shaded leaf photosynthesis, respectively.

2.2 | CI datasets

Three publicly available global CI datasets (Table 1) at 500m spatial resolution that we can find were used in this study. The three CI products (UofT-CI, CAS-CI, and BNU-CI) were generated based on the empirical relationship between CI and the index of normalized difference in reflectance between the hotspot (the direction where solar radiation and view directions coincide and no shadows are observed) and darkspot (the direction where maximum shadowing and minimum reflectance are observed) (normalized difference hotspot and darkspot [NDHD]; Chen et al., 2005; Leblanc et al., 2005). However, differences were founded in the three datasets because of their used BRDF models and sun zenith angle (SZA) settings, which can cause substantial differences in calculated NDHD and thus CI (Fang, 2021; Wei et al., 2019; Wei & Fang, 2016). For UofT-CI, He et al. (2012) corrected and reproduced MODIS-derived hotspot reflectance based on the empirical relationship between MODIS and POLDER hotspot observations and used SZA values of 0° and 47.7° for estimating the hotspot and darkspot reflectance in the BRDF model of RossThick-LiSparse Reciprocal (RTLSR). For CAS-CI, Wei et al. (2019) corrected the hotspot of MODIS with the method in He

et al. (2012), and used observed SZA to estimate NDHD through the RTLSR model. For BNU-CI, Jiao et al. (2018) adopted a backup algorithm to reprocess potential outliers of CI with a prescribed physical range, and used the hotspot-adjusted version (i.e., RTCLSR) of the RTLSR model to estimate the hotspot and darkspot reflectance at 45° both in the backward and forward directions for NDHD calculation. In addition, UofT-CI and BNU-CI datasets were based on the version 5 of MODIS BRDF product (MCD43A1), while CAS-CI dataset was based on that of version 6 with improved inversion quality and ability to detect temporal changes (Wang, Schaaf, et al., 2018).

We scaled up each CI dataset to the resolution of the model run with CLM prescribed plant functional types (PFTs; Bonan et al., 2002). Using Google Earth Engine (Gorelick et al., 2017), we first derived 500m resolution CLM PFT dataset from 500m MODIS land cover type dataset (MCD12Q1; Friedl & Sulla-Menashe, 2015) and WorldClim V1 ~1 km (linearly interpolated to 500m) monthly temperature and precipitation dataset (Hijmans et al., 2005) based on the described rules in Bonan et al. (2002) and Hao et al. (2022). Then we used the derived CLM–PFT dataset to upscale the CI dataset from 500m resolution to the resolution of model run by averaging CI values at finer resolution with the same PFT (Hao et al., 2022). Given the temporal coverage of UofT-CI dataset and generally small interannual variation of CI (He et al., 2016; Wei et al., 2019), we used the CI in 2006 for subsequent analyses (Braghiere et al., 2019). Same to the UofT-CI dataset, we calculated the yearly median of the BNU-CI and CAS-CI datasets using their raw CI datasets. The CI information over space and different biome types was shown as Figure 1. We analyzed the across-data CI differences in Section 3.1, and analyzed the impacts of CI seasonal variations on GPP using monthly CAS-CI and BNU-CI datasets in Section 3.4.

2.3 | Model setup and evaluation

We ran CLM5 with the prescribed satellite phenology (SP) mode at the 1.9°×2.5° spatial resolution. The Global Soil Wetness Project (GSWP3) dataset (Dirmeyer et al., 2006) was used as climate forcing, including 3-h total incident solar radiation, incident longwave radiation, total precipitation, surface air pressure, air temperature, wind speed, and specific humidity. In the SP mode, prescribed LAI from the MODIS LAI product (Myneni et al., 2002) is used (Lawrence & Chase, 2007). Albeit the uncertainty in MODIS LAI product when

TABLE 1 Details of the three global CI products used in the study

Dataset	BRDF model	Solar zenith angle	MODIS BRDF product	Temporal coverage	References
UofT-CI	RTLSR	(hotspot SZA = 0°) and (darkspot SZA = 47.7°)	MCD43A1 version 5	2006	He et al. (2012)
BNU-CI	Hotspot adjusted, RTCLSR	SZA = 45°	MCD43A1 version 5	2000–2019	Jiao et al. (2018)
CAS-CI	RTLSR	Observed SZA	MCD43A1 version 6	2001–2019	Wei et al. (2019)

Abbreviations: BRDF, bidirectional reflectance distribution function; CI, clumping index; MODIS, Moderate Resolution Imaging Spectroradiometer; SZA, solar zenith angle.
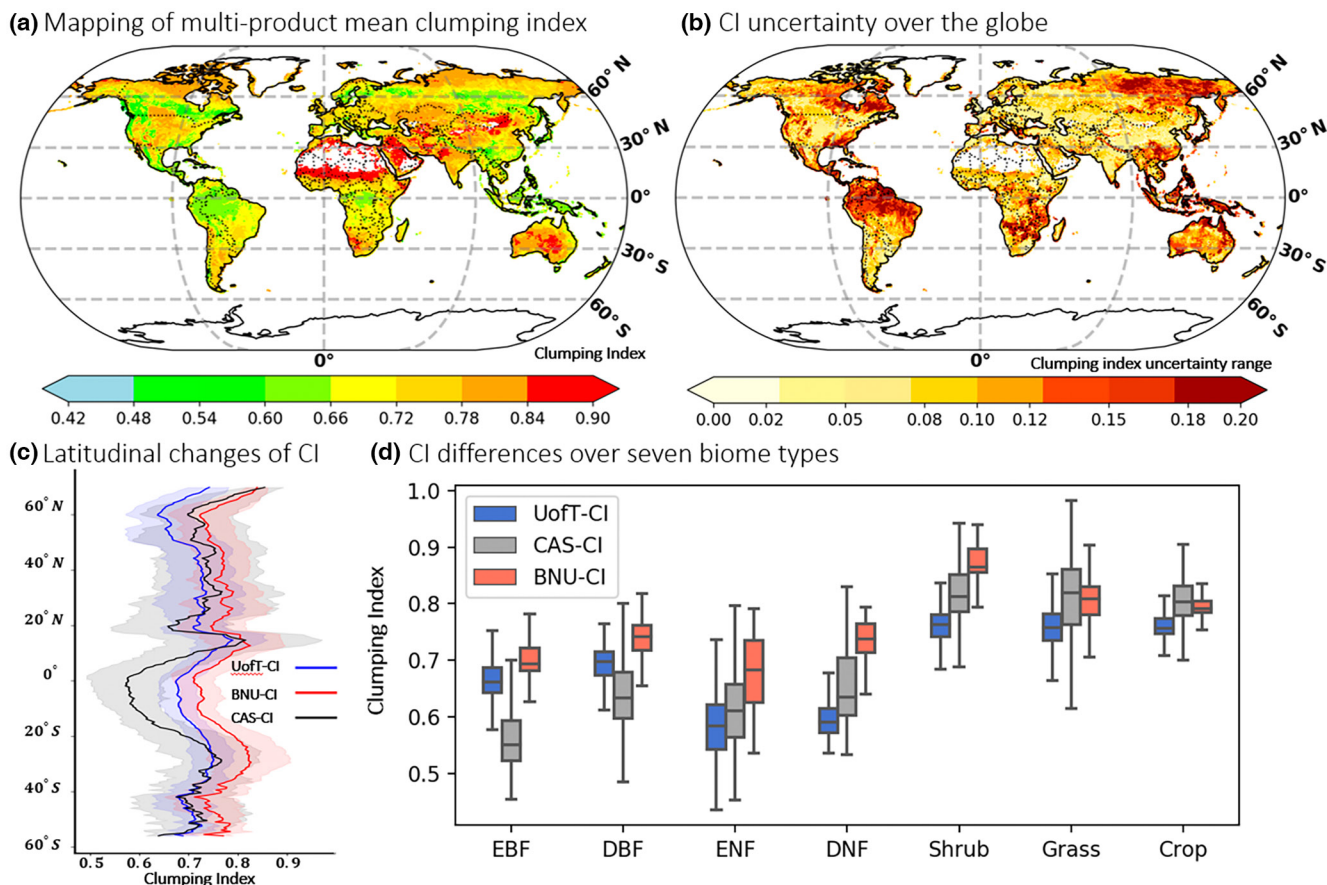
(a) Mapping of multi-product mean clumping index

(b) CI uncertainty over the globe

(c) Latitudinal changes of CI

(d) CI differences over seven biome types

FIGURE 1 Multi-product mean CI (a) and uncertainty range of global CI (b); the latitudinal mean (lines) and standard deviation (shades) of three CI datasets (c), and the distributions of CI values over seven biome types over the globe (d). Map lines delineate study areas and do not necessarily depict accepted national boundaries. CI, clumping index.

compared with that of fields measurement, its retrieval algorithm considered CI (Knyazikhin, 1999; Knyazikhin et al., 1998), and MODIS LAI is generally closer to true LAI rather than effective LAI (i.e., $\Omega \times$ LAI) (Yan et al., 2016). Therefore, we considered CLM5-SP simulations with prescribed LAI but without CI as the baseline case that ignored CI effects. Hereafter, we referred to the original baseline model as CLM5 ($\Omega = 1$) and the modified model using the prescribed annual median CI as CLM5-CI, respectively. Similar to previous studies (Braghiere et al., 2019; Chen et al., 2012), the CI impacts were calculated as the differences between the results from the two model versions (i.e., CLM5-CI—CLM5). To separate the impacts on GPP due to changed canopy energy regime and nitrogen distribution, we also turned off the CI-induced nitrogen distribution changes in CLM5-CI (referred as CLM5-CI-noN). Therefore, the difference between results of CLM5-CI-noN and CLM5 was regarded as the CI impacts on GPP through changed canopy energy regime, and the difference between CLM5-CI and CLM5-CI-noN was regarded as the CI impacts on GPP through changed nitrogen distribution and thus V_{cmax}. In addition, we also investigated the impacts of CI seasonal variations on GPP by calculating the differences between the estimated GPP using monthly varied and annual median CI information. For each experiment, model outputs were aggregated to annual values as we focused on CI impacts on annual GPP

estimates. Each model simulation was performed for 11 years from 2000 to 2010, and we analyzed the last 5-year outputs from 2006 to 2010 to eliminate the impacts of model initialization.

The uncertainty of CI and its impacts on canopy radiative transfer and photosynthesis were evaluated over seven biome types, including evergreen broadleaf forest (EBF), deciduous broadleaf forest (DBF), evergreen needleleaf forest (ENF), deciduous needleleaf forest (DNF), shrubs, grasses, and crops. The uncertainty range of CI was defined as the difference between the maximum CI and the minimum CI among the three CI datasets. The uncertainty range of CI-induced impacts on canopy radiation and photosynthesis was defined as the difference between the maximum and minimum CI-induced changes.

2.4 | Benchmarking GPP dataset

We used the GOSIF-GPP (Li & Xiao, 2019) and FluxCom GPP (Jung et al., 2017; Tramontana et al., 2016) products as the benchmarking datasets to evaluate the GPP estimates from CLM simulations. The GOSIF-GPP dataset is derived based on the solar-induced chlorophyll fluorescence (SIF) observed by the Orbiting Carbon Observatory-2 (OCO-2) and its linear relationship with GPP (Li

et al., 2018; Li & Xiao, 2019); while the FluxCom GPP is derived from multiple machine learning algorithms (i.e., Random Forest, Artificial Neural Network, and Multivariate Adaptive Regression Splines) trained on site tower-based carbon fluxes along with meteorological measurements and satellite data as inputs (Jung et al., 2017; Tramontana et al., 2016). Both datasets have been widely used in terrestrial carbon budget estimates (Mohammed et al., 2019; Ryu et al., 2019), and are purely data-driven products, thus avoiding any preset assumptions regarding canopy radiative transfer (i.e., with or without consideration of CI).

3 | RESULTS

3.1 | Considerable variations of CI over space and different biome types

Figure 1a showed the global distribution of multi-product mean CI. Statistics of three product ensemble mean showed that the most clumped biome types were EBF (0.64 ± 0.03) (mean $\pm$ 1SD) and ENF (0.63 ± 0.06), followed by DNF (0.66 ± 0.04) and DBF (0.69 ± 0.04), while shrub (0.81 ± 0.04) was the least clumped biome type. Generally, forests were more clumped than shrubs, grasses, and crops. Considerable uncertainty was observed across the three CI datasets over the globe (Figure 1b), and further intercomparison of three CI products revealed substantial differences in CI distribution over space (Figure 1c) and seven biome types (Figure 1d).

The three CI datasets showed similar latitudinal patterns but their magnitudes differed (Figure 1c). CAS-CI had the lowest CI values (0.66 ± 0.07) in tropical ($23.5°$ S–$23.5°$ N) regions compared with the values of BNU-CI (0.76 ± 0.03) and UofT-CI (0.71 ± 0.03). The CI values in temperate and frigid regions (northern of $23.5°$ N and southern of $23.5°$ S) were 0.72 ± 0.02 in UofT-CI, 0.80 ± 0.06 in BNU-CI, and 0.78 ± 0.02 in CAS-CI, respectively. Overall, the values of BNU-CI were higher than those of the two others particularly in tropical zones (Figure 1c). CI values of the three datasets all followed the order that forest was more clumped than other biome types (i.e., shrubs, crops, and grasses) (Figure 1d), however, in different forest types, significant differences (two-tailed t test, $p < .05$) were found among the three datasets. ENF and DNF were most clumped forest types in UofT-CI while EBF was the most clumped one in CAS-CI, and CI values showed relatively similar magnitude across EBF, DBF, ENF, and DNF in BNU-CI (Figure 1d). The impacts of those across-dataset CI differences on canopy radiation transfer and photosynthesis need to be explored.

3.2 | Opposite impacts of clumping on light absorption in sunlit and shaded canopies

By definition, sunlit canopy absorbs direct and diffuse radiation, while shaded canopy only absorbs diffuse radiation. Introducing CI generally decreases (increases) sunlit (shaded) leaf area (Equations 3 and

4, $\Omega < 1$), which also adjusts sunlit and shaded canopy absorbed direct and diffuse radiation. The FAPAR of sunlit and shaded canopy is closely linked to LAI and CI. Figure 2a–c respectively showed how the absorption of direct PAR in sunlit canopy, diffuse PAR in sunlit canopy, and diffuse PAR in shaded canopy (i.e., $\mathrm{FAPAR_{sun,dir}}$, $\mathrm{FAPAR_{sun,dif}}$, and $\mathrm{FAPAR_{sha,dif}}$, respectively) changed with LAI in CLM5. FAPAR increases with LAI and saturates at some point (Figure 2a–c; Bonan, 2019; Myneni et al., 2002). With the same LAI, a more clumped canopy (lower CI) will decrease sunlit LAI (Chen et al., 2012), and the absorbed direct and diffuse radiation on sunlit canopy (Figure 2a,b). In contrast, for shaded canopy, leaf clumping increases FAPAR of diffuse radiation especially for high LAI biomes (e.g., tropical forest) (Figure 2c), because diffuse radiation can penetrate deeper than direct radiation into the canopy where the leaves are light-limited (Braghiere et al., 2019). Compared to direct and diffuse radiation in sunlit canopy, absorption of diffuse radiation in shaded canopy increased and tended to be less saturated with larger LAI values (Figure 2c; Durand et al., 2021; Mercado et al., 2009; Williams et al., 2016).

At the global scale, after accounting for the CI effects, the mean $\mathrm{FAPAR_{sun,dir}}$ (Figure 2d) and $\mathrm{FAPAR_{sun,dif}}$ (Figure 2e) consistently decreased with three CI datasets, and the decreased values were up to 9.4%–14.8% and 22.8%–33.7% of their raw values across the different biome types (Figure S1a,b). Oppositely, $\mathrm{FAPAR_{sha,dif}}$ consistently increased (Figure 2f) up to 3%–18% (Figure S1c) across different biomes. The influence of CI on shaded canopy was most prominent in the tropical area (Figure 2f) for the EBF biome type, where the $\mathrm{FAPAR_{sha,dif}}$ values averagely increased by 14%–18% considering clumping effects (Figure S1c).

3.3 | Contrasting changes in sunlit and shaded canopy photosynthesis

Accounting for CI decreased FAPAR in sunlit canopy resulted in ~6% lower in canopy absorbed total PAR (Figure S2), and the decrease could be up to 18% in some regions. Meanwhile, decreased (increased) sunlit (shaded) leaf area fraction decreased (increased) nitrogen content allocated in sunlit (shaded) canopy and thus V_{cmax} (Equations 9 and 10). Consequently, through changing canopy absorbed energy, the incorporation of CI increased (decreased) shaded (sunlit) canopy GPP globally by $5.8 \, \mathrm{PgC \, year^{-1}}$ ($6.8 \, \mathrm{PgC \, year^{-1}}$) (Figure 3a,b); through changing nitrogen distribution, GPP was increased (decreased) by $2.8 \, \mathrm{PgC \, year^{-1}}$ ($0.8 \, \mathrm{PgC \, year^{-1}}$) in shaded (sunlit) canopy (Figure 3c,d). The impacts of CI-induced changes of energy absorption on GPP were ~2.1 and ~8.5 times as large as that caused by nitrogen distribution for shaded and sunlit canopy, respectively. In combination of energy and nitrogen distribution changes together, sunlit canopy photosynthesis decreased globally (Figure 3e) while shaded canopy photosynthesis increased, especially in tropical forests (Figure 3f). The degree to which photosynthesis of the entire canopy will change is contingent on the balance of increase in shaded canopy photosynthesis against the decrease in sunlit canopy photosynthesis.
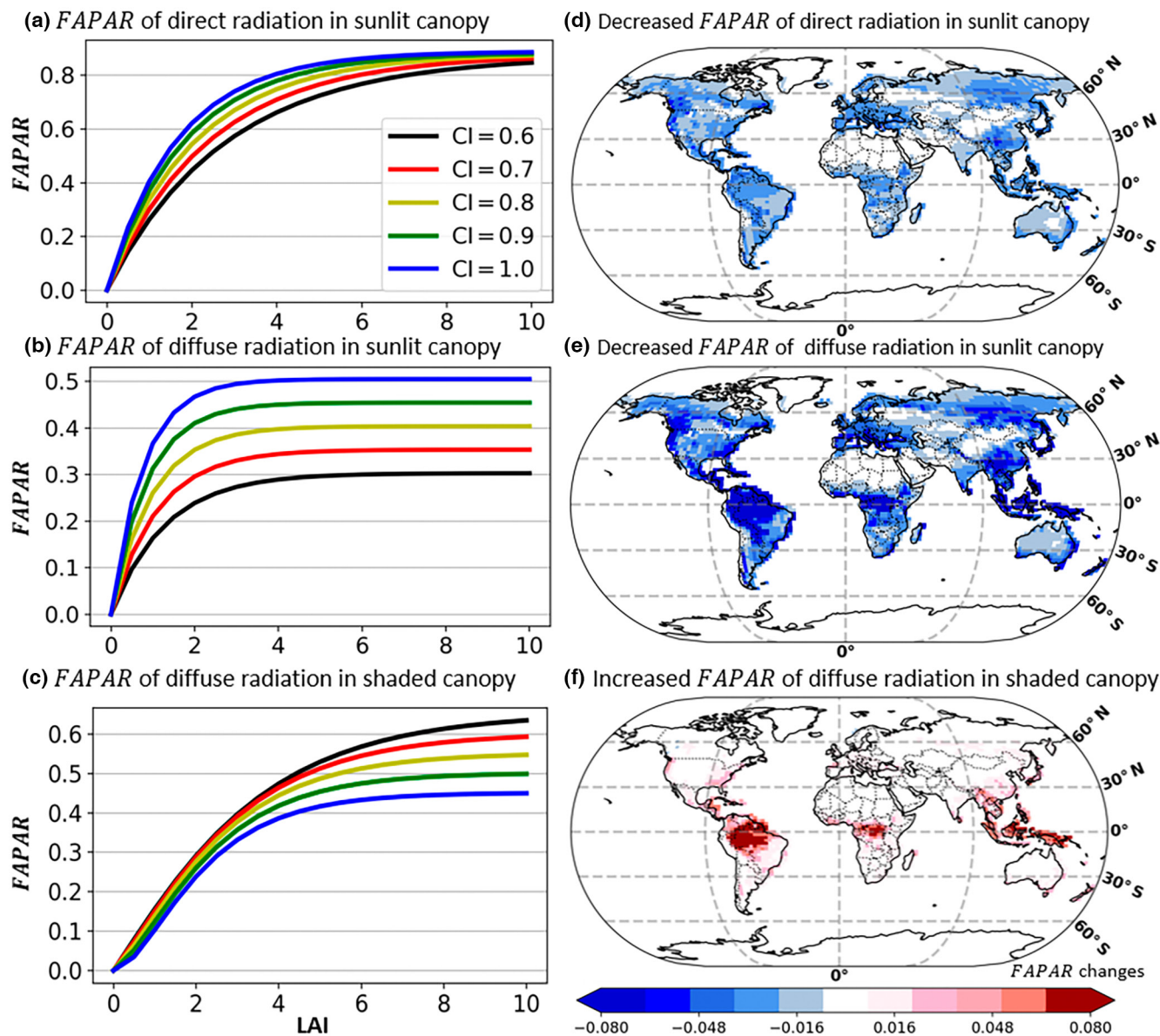
FIGURE 2 CI induced changes in FAPAR in relation to LAI for direct radiation (a) and diffuse radiation (b) in sunlit canopy, and diffuse radiation in shaded canopy (c). Mean changes of FAPAR for direct radiation in sunlit canopy (d), diffuse radiation in sunlit canopy (e), and diffuse radiation in shaded canopy (f) at the global scale. (a–c) are generated using the two-stream model in CLM5 but with prescribed LAI, CI, and optical parameter values (leaf reflectance and transmittance are 0.10 and 0.05, respectively; optical depth of direct beam and diffuse radiation are 0.58 and 0.70, respectively; upscatter parameter for diffuse and direct radiation are 0.54 and 0.46, respectively (Bonan, 2019). Deeper blue (red) color represents lower (higher) FAPAR after accounting for clumping in (d–f). Map lines delineate study areas and do not necessarily depict accepted national boundaries. CI, clumping index; FAPAR, fraction of absorbed photosynthetically active radiation; LAI, leaf area index.

At the global scale, compared to the CLM5 without clumping, the amount of sunlit canopy photosynthesis with CI decreased by 5.9–7.2 PgC year^{-1} while shaded canopy photosynthesis increased by 6.9–8.2 PgC year^{-1} (Figure 4). CI-induced increase in shaded canopy photosynthesis overwhelmed sunlit canopy decreased photosynthesis, likely due to the higher LUE of shaded canopy than that of sunlit canopy (Figure S3; Braghiere, Quaife, et al., 2020; Durand et al., 2021; Mercado et al., 2009; Williams et al., 2016). As a result, carbon uptake over the entire canopy with CI globally increased by 1.0 ± 0.12 PgC year^{-1}. CI-induced photosynthesis changes were the most prominent over the EBF biome type with greater LAI values

(Figure 4). Specifically, the shaded canopy GPP increased by 3.4–4.8 PgC year^{-1} and sunlit canopy GPP decreased by 2.3–3.6 PgC year^{-1} in EBF, which dominated CI-induced global GPP changes.

3.4 | CI-induced changes in canopy photosynthesis and its uncertainty

At the global scale, a systematic bias of ~1.0 PgC year^{-1} would be expected in estimated GPP if CI effects were ignored. The bias was most prominent in tropical regions (Figure 5a), and CI-induced
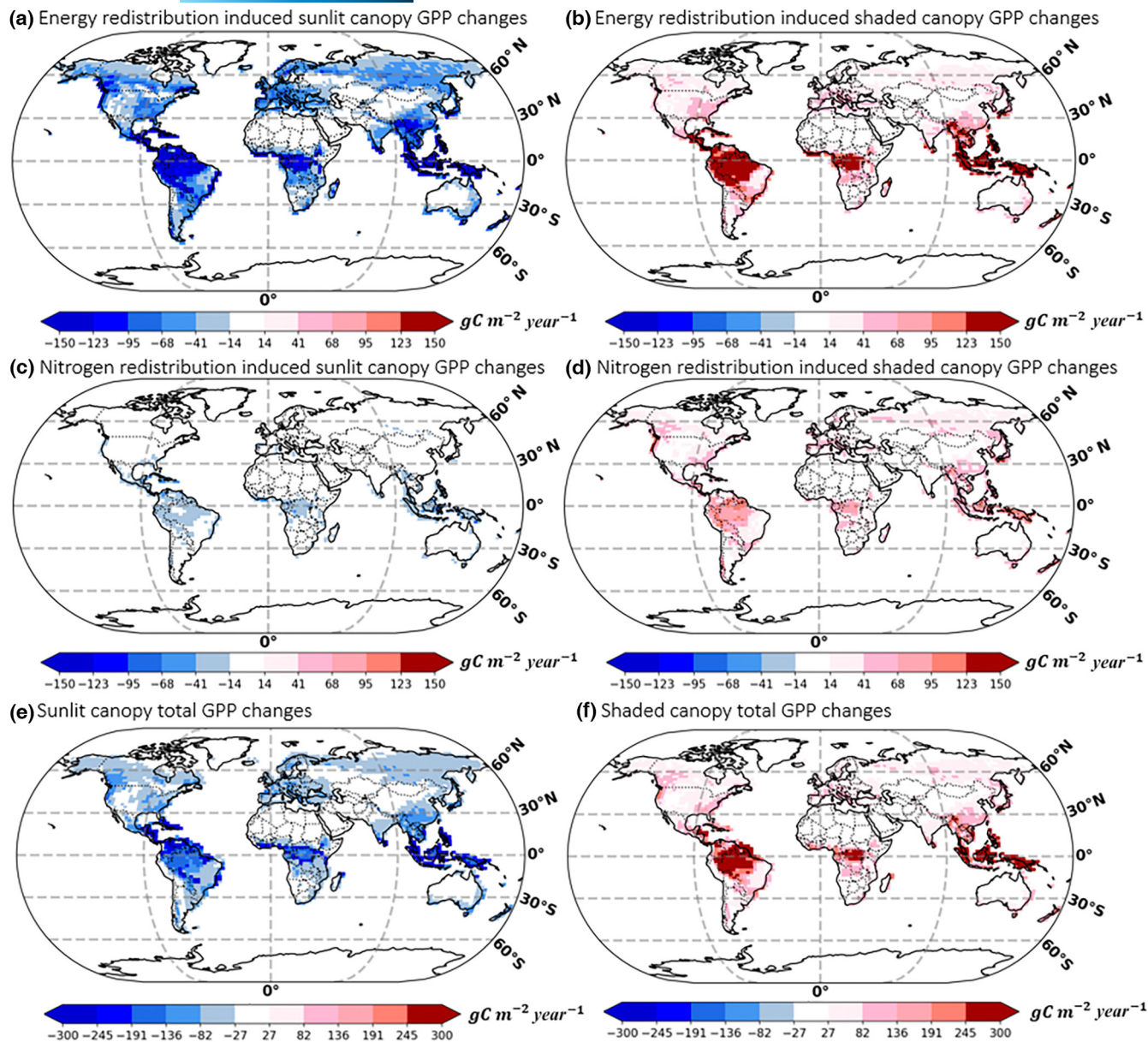
FIGURE 3 CI induced GPP changes in sunlit and shaded canopy. (a, b) Are CI-induced GPP changes through changing energy absorption of sunlit and shaded canopy, respectively. (c, d) Are CI-induced GPP changes through changing nitrogen distribution in sunlit and shaded canopy, respectively. (e, f) Are CI-induced total GPP changes in sunlit and shaded canopy, respectively. Deeper blue (red) color represents lower (higher) GPP after accounting for clumping. Map lines delineate study areas and do not necessarily depict accepted national boundaries. CI, clumping index; GPP, gross primary production.

regional differences in estimates of GPP can be up to 10% (Figure 5b). Satellite-based observations of CI enable spatially varied representation of CI effects in CLM5, but CI itself is with considerable uncertainties (Figure 1). The uncertainty of CI from the different products propagated to GPP estimates (Figure 5c), which is comparable with up to 50% of GPP interannual variations (tropical area in Figure 5d).

Considering CI but ignoring its seasonal variations can increase estimation of global GPP by ~0.14 PgC year^{-1}, with the largest differences (~4%) occurred in the boreal forest region (Figure 5e). The magnitude of CI seasonal variation induced GPP changes was much smaller than that of GPP changes in tropical forests induced by the across-data CI uncertainty (Figure 5f). Therefore, while leveraging

satellite-derived observations of CI can reduce CI-induced bias in estimated GPP, the uncertainty of CI needs to be further narrowed.

3.5 | Comparison with satellite-based observations

Model estimates of GPP with and without CI were respectively compared with two benchmarking datasets: GOSIF-GPP and FluxCom-GPP. Figure 6a showed the difference in the absolute bias (i.e., the absolute value of the reference GPP data minus the modeled GPP) between CLM5-CI and GOSIF-GPP, and CLM5 and GOSIF-GPP. Deeper blue (red) color represented lower (higher) bias between

FIGURE 4 Gross primary production changes in sunlit and shaded canopy over different biome types.
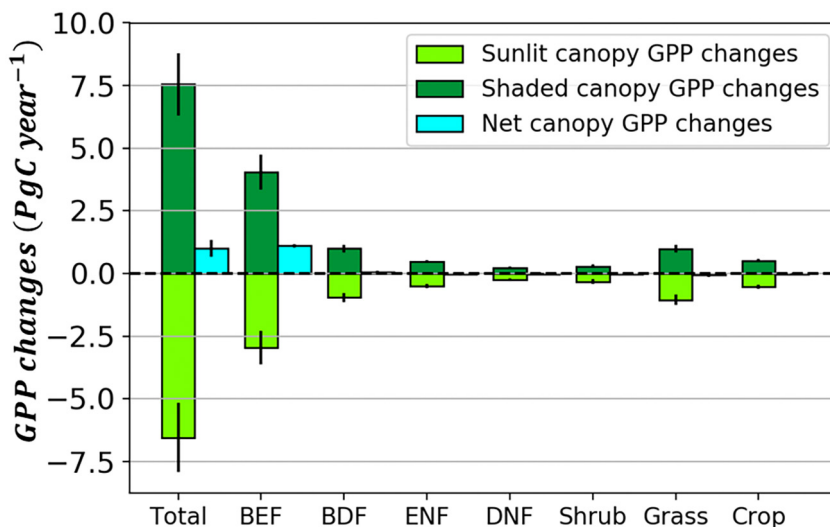
modeled GPP and GOSIF-GPP after accounting for clumping. With clumping, the discrepancy between modeled GPP and GOSIF-GPP was generally smaller, especially for the tropical region (Figure 6a). Specifically, compared to the absolute bias between CLM5 and GOSIF, the mean absolute bias between CLM5-CI and GOSIF decreased mostly in EBF (Figure 6b) with bias decreased by 91.4–115.5 $gCm^{-2}year^{-1}$ (−19.3% to −24.4%). Similar results (Figure S4) were acquired using the FluxCom-GPP as the benchmarking dataset.

4 | DISCUSSION

Vegetation clumping is an integral part of canopy structure that determines canopy radiation transfer (Bonan, 2019), photosynthesis (Braghiere et al., 2019; J. M. Chen et al., 2012), and hydrological processes (B. Chen et al., 2016, 2021). Without accounting for clumping, sunlit leaf area and sunlit canopy absorbed radiation are overestimated, while canopy radiation transmittance, shaded leaf area, and shaded canopy absorbed radiation are underestimated. This results in biases in estimated sunlit/shaded canopy GPP at regional and global scales. Satellite-based observations of CI enable spatially resolved representation of clumping in TBMs, however, CI is not considered in the state-of-the-art CLM5 (nor in other TBMs in Table S1), and large uncertainty across existing CI datasets should also be considered. This study included CI in CLM5 and systematically analyzed the extent to which sunlit/shaded canopy absorbed direct/diffuse radiation and photosynthesis will be changed when considering clumping and its uncertainty. We found CI-induced increase in GPP in shaded canopy overwhelmed the decreased GPP in sunlit canopy globally, and caused a net $1.0\pm0.12\,PgCyear^{-1}$ increase in GPP.

4.1 | Comparison with previous studies on clumping induced bias in GPP estimates

The CI impact on canopy photosynthesis found in our study is consistent with the results in multiple previous site-level studies.

Walcroft et al. (2005) found a 11% decrease in canopy radiation absorption but 12% increase in canopy photosynthesis with a considerable enhancement of canopy LUE after accounting for clumping at a rainforest site. Baldocchi and Wilson (2001) found a 12.5% increase in canopy photosynthesis when involving CI at a broadleaved forest site and also showed amplified positive impacts of clumping on canopy photosynthesis when the leaf area increased. Similar results were also shown in Wang and Polglase (1995) and Braghiere, Quaife, et al. (2020). Braghiere, Quaife, et al. (2020) showed an increase in GPP with clumping in two forest sites. Our results also showed varied influence of clumping on canopy photosynthesis, and the most prominently positive impacts of clumping were in tropical regions or in the EBF with greater leaf areas (Figure 4). A few previous studies have reported their findings on the CI impacts on global GPP (Table S2). With a coarse resolution (~6km) of POLDER derived CI dataset, Ryu et al. (2011) and Chen et al. (2012) showed reduced GPP values (1.5 vs. 15.88 PgCyear^{-1}) using the BESS and BEPS model, respectively. Using a higher-resolution (~500m) CI dataset, Braghiere et al. (2019) showed increased GPP (5.53 PgCyear^{-1}) with the JULES model. Braghiere et al. (2019) explained the main reason for the opposite CI impacts on GPP was the greater penetration of light into lower layers that were light-limited and boosted photosynthesis. Our CLM5-based results were opposite to the Ryu's and Chen's results but consistent with Braghiere's results, as we have shown that the consideration of CI increased global GPP, mostly in the tropical forests. While it is challenging to reproduce Ryu's and Chen's model experiments, we could discuss their differences in the processes related to canopy energy absorption and distribution, as these are the first order and most direct impacts of CI.

Vegetation clumping firstly impacts global photosynthesis through adjusting canopy light environment which consequently alters absorbed energy in sunlit and shaded canopies (Chen et al., 2012). Modeling analyses showed that the diffuse radiation fraction (DRF) of solar radiation, LAI, and CI all interactively affected the energy absorption and distribution in the canopy (Figure 7). When the DRF was high (e.g., DRF = 100%, Figure 7a) and LAI was large, the FAPAR of shaded canopy was generally larger than that of sunlit canopy
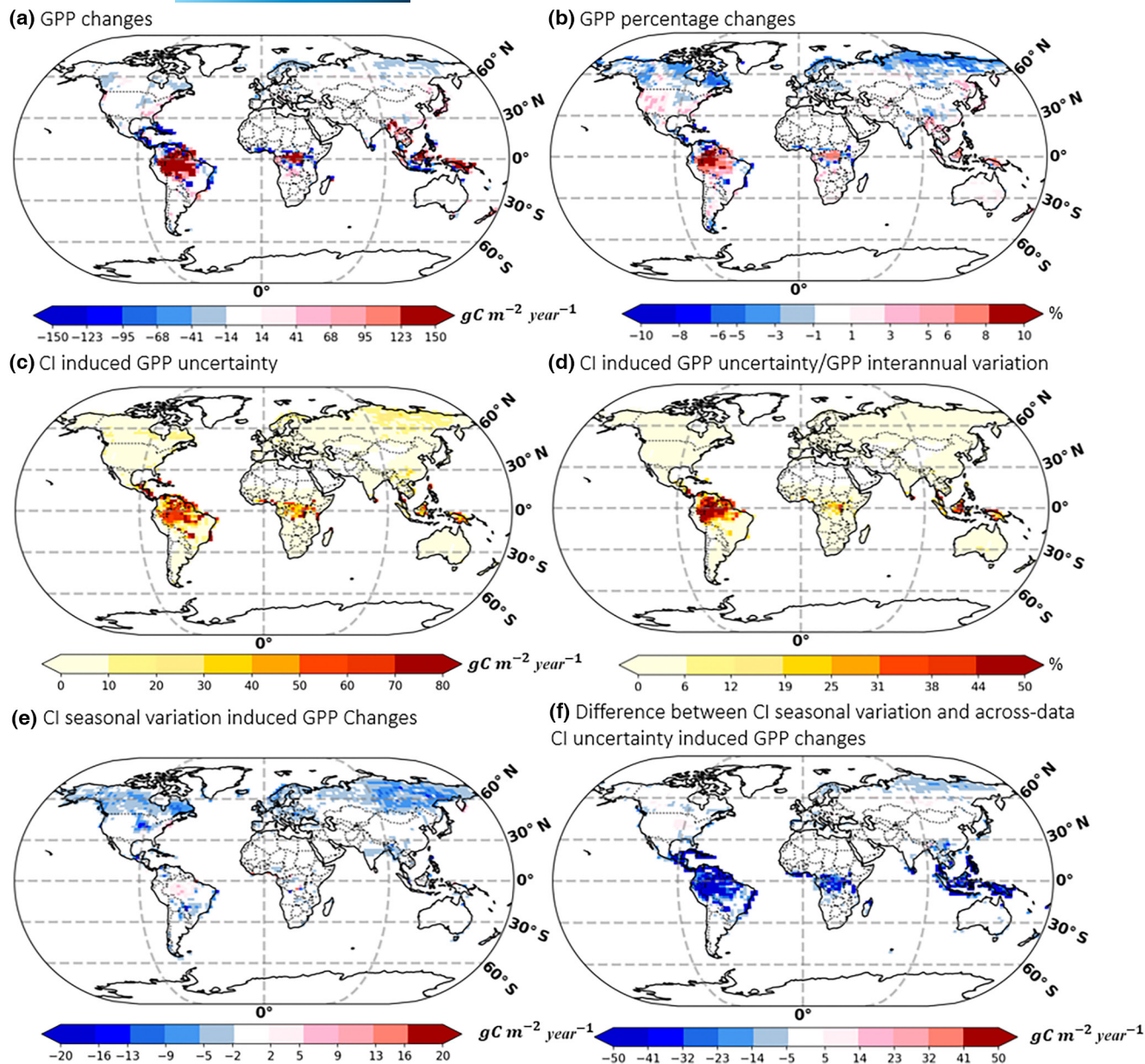
(a) GPP changes

(b) GPP percentage changes

(c) CI induced GPP uncertainty

(d) CI induced GPP uncertainty/GPP interannual variation

(e) CI seasonal variation induced GPP Changes

(f) Difference between CI seasonal variation and across-data CI uncertainty induced GPP changes

FIGURE 5 CI induced changes in GPP in magnitude (a) and percentage (b). The uncertainty of GPP by using different CI datasets is shown in (c) and its relative values to GPP interannual variations is shown in (d). (e, f) Illustrate the impacts of CI seasonal variation on GPP changes and their spatial pattern in relative to (c). Deeper blue (red) color represents lower (higher) GPP after accounting for clumping in (a, b). Deeper blue (red) color represents lower (higher) GPP when considering CI seasonal variation relative to that of using CI median in (e), or lower (higher) than that of GPP changes induced by across-data CI uncertainty in (f). Map lines delineate study areas and do not necessarily depict accepted national boundaries. CI, clumping index; GPP, gross primary production.

and increased faster with LAI when CI was small; at low LAI, CI-induced changes of FAPAR in shaded canopy were limited and much smaller than that in sunlit canopy. At the medium level of DRF (e.g., DRF = 50%, Figure 7b), the impacts of CI on FAPAR in shaded canopy were weaker than that under high DRF conditions. When DRF was low (e.g., DRF = 0%, Figure 7c), CI showed limited positive impacts on FAPAR in shaded canopy but much stronger negative impacts on FAPAR in sunlit canopy. As a result, when DRF was low (Figure S5) and LAI is small (blue regions in Figure 5a,b), sunlit canopy dominated canopy total FAPAR and thus CI decreased GPP. In contrast, with higher DRF (Figure 5a,b relative to that in Figure S5) and larger

LAI (e.g., tropical forest in Figure 5a,b), CI increased FAPAR and GPP in shaded canopy dominated the GPP changes. Therefore, the use of different LAI [i.e., VEGETATION LAI product in Chen et al. (2012) versus different versions of MODIS LAI products in Ryu et al. (2011) and this study] and CI [i.e., ~6km resolution POLDER CI in Chen et al. (2012) and Ryu et al. (2011) vs. ~500m MODIS-based multiple CI products of this study] datasets could be an important reason for the inconsistencies among our study and previous studies.

Meanwhile, different diffuse versus direct radiation partitioning methods were applied in CLM5, BEPS (Chen et al., 2012), and BESS (Ryu et al., 2011). Therefore, the DRFs estimated by the three
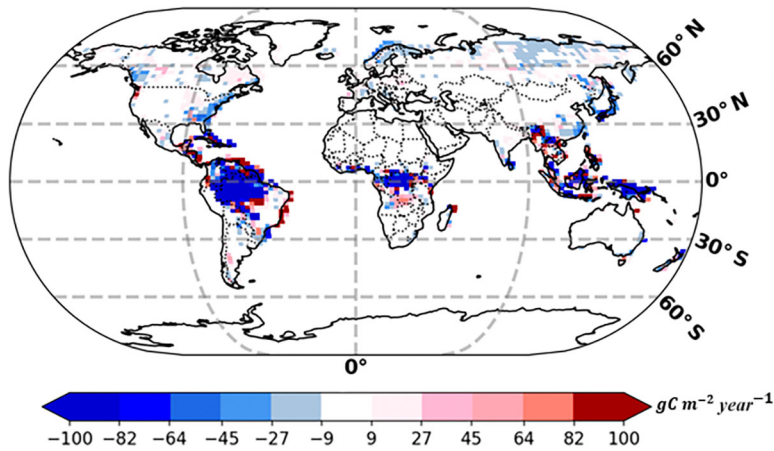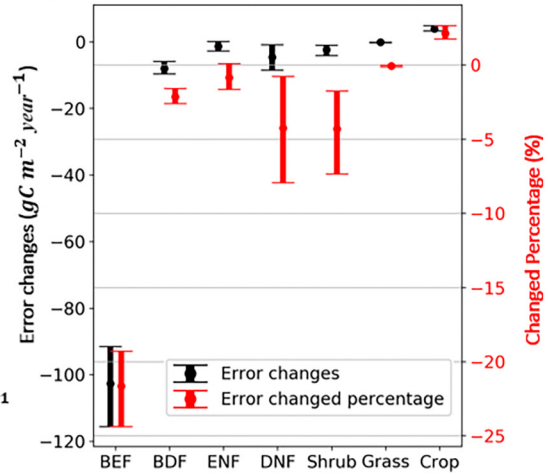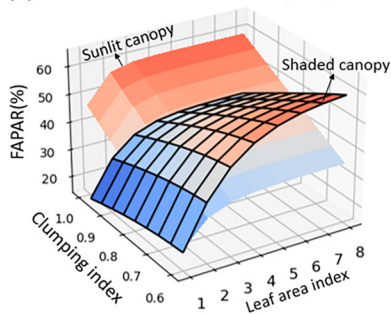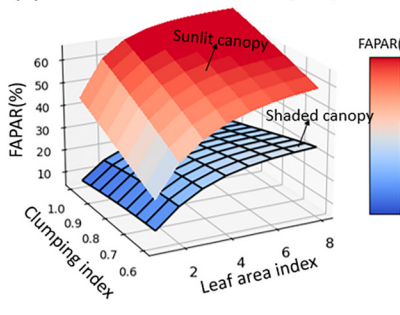
FIGURE 6 Difference of absolute bias in gross primary production between (CLM5-CI—GOSIF) and (CLM5—GOSIF) at the global scale (a) and over different biome types (b). Deeper blue (red) color represents lower (higher) bias after accounting for clumping in (a). Map lines delineate study areas and do not necessarily depict accepted national boundaries.
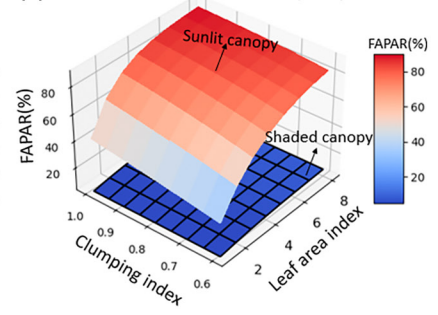

FIGURE 7 The interactive impacts of diffuse radiation fraction, CI, and LAI on the fraction of absorbed photosynthetically active radiation in sunlit and shaded canopy. (a–c) Are generated using the two-stream model in CLM5 but with prescribed LAI, CI, diffuse radiation fraction, and optical parameter values (leaf reflectance and transmittance is 0.10 and 0.05; optical depth of direct beam and diffuse radiation is 0.58 and 0.70; upscatter parameter for diffuse and direct radiation is 0.54 and 0.46 (Bonan, 2019). CI, clumping index; LAI, leaf area index.

models could be different, resulted in different CI impacts on FAPAR (Figure 7) and thus GPP. For example, according to Chen et al. (2012), the DRF in BEPS could be ~5%–10% lower than site observations and its calculation method tended to underestimate DRF for air masses with large aerosol contents. The DRF of CLM5 was ~9%–10% higher than that of BEPS (Figure S6). A higher DRF would enhance the positive impact of CI on shaded canopy FAPAR (Figure 7) and GPP (Durand et al., 2021; He et al., 2018; Yan et al., 2019).

Another reason for the inconsistency could be the model-specific consideration of the leaf nitrogen distribution in vegetation canopy. The CLM5, BEPS, and BESS all assumed that the leaf nitrogen distribution in sunlit and shaded canopy was determined by the sunlit–shaded leaf area fraction (Bonan, 2019; Chen et al., 2012; Ryu et al., 2011). CI increased shaded leaf area fraction and the nitrogen allocated on shaded canopy, which considerably increased shaded canopy GPP (Figure 3d). Such impacts were likely underestimated in Ryu et al. (2011) and Chen et al. (2012). Ryu et al. (2011) did not consider CI impacts on nitrogen distribution in sunlit–shaded canopy (see Eq. 33 in Ryu et al. (2011)), while the mean fraction of leaf nitrogen content on shaded canopy in

Chen et al. (2012) was underestimated (see Eq. B6 in Chen et al. (2012)) relative to this study (Equation 10), which could underestimate the positive impacts of CI on shaded and thus entire canopy GPP. In addition, other differences can also be a part of the reasons for the differences among studies, including the forcing datasets (e.g., NCEP vs. GSWP3 climate datasets), model structures (e.g., different canopy radiative transfer schemes) (Bonan, 2019; Braghiere et al., 2019; Chen et al., 2012; Goudriaan, 1977; Norman & Welles, 1983), and model parameterizations (e.g., different nitrogen extinction coefficient settings) (Chen et al., 2012; Lawrence et al., 2019; Ryu et al., 2011).

4.2 | Reducing clumping induced bias in past, present, and future model simulations

Our results along with previous studies (Braghiere et al., 2019; Chen et al., 2012; Ryu et al., 2011) suggested significantly systematic bias in estimated GPP when ignoring CI effects. The bias also likely exists in other TBMs (Table S1) that assume a random distribution of leaves

within a vegetation canopy. We found substantial differences of CI magnitude within each biome type (Figure 1), implying that spatially resolved representation of CI is needed instead of a biome-specific CI value setting strategy (Loew et al., 2014). Without accounting for the clumping effects, the systematic bias in canopy radiation transfer and photosynthesis should persist through past–present–future TBM and ESM simulations.

During the past two decades, smaller interannual variation (−0.007/decade) of CI was observed (Wei et al., 2019), and the clumping induced bias in photosynthesis was most pronounced in tropical regions with high LAI values. However, future anthropogenic warming and CO_2 fertilization-induced global greening (Piao et al., 2006, 2020) may amplify the CI effects in forests with increased leaf area and absorbed diffuse radiation (Figure 2c). Meanwhile, long-term climate change and land use land cover changes may significantly alter land surface characteristics at a century scale (Hoffmann et al., 2021), and consequently change the spatial distributions of CI and its impacts on photosynthesis. Mitigating CI-induced offset therefore, also requires reasonable representation of CI for past and future climate simulations when CI observations are not available.

4.3 | Directions for future research

This study mainly focuses on the CI impacts on photosynthesis through changing canopy light conditions. Beyond that, CI also affects surface water and energy cycle (B. Chen et al., 2016, 2021) which could in turn exert indirect and longer term effects on GPP. For example, including CI into the model increased solar energy reaching the ground (Baldocchi & Wilson, 2001; Braghiere et al., 2019; Braghiere, Quaife, et al., 2020; Law et al., 2001) and thus enhanced the latent heat flux for evaporation broadly (Figure S7a). The transpiration latent heat flux was enhanced mainly in tropical forests (Figure S7b), suggesting higher stomata conductance and photosynthesis in the tropical forests (Chen & Zhuang, 2014; Yuan, Zhu, Riley, et al., 2022). Due to increased evaporation and transpiration, we observed a total global net water loss through evapotranspiration with the most significant loss occurred in the tropical regions (Figure S7c). The water-stress factor β that linearly scales GPP (a smaller β would result in a smaller GPP) (Braghiere, Gérard, et al., 2020; Verhoef & Egea, 2014) in the model generally decreased at a very small magnitude due to the use of CI (Figure S8). Therefore, CI increased stomatal conductance and GPP but also increased water loss which may limit photosynthesis especially under water-limited conditions (Yuan, Zhu, Riley, et al., 2022). The long-term impacts of CI on GPP need further exploration especially considering water-limited conditions.

Similar to many other models including those in Ryu et al. (2011) and Chen et al. (2012), CLM5 uses a single-layer canopy assumption. We found that incorporation of CI enhanced solar energy absorption and nitrogen allocation and thus photosynthesis in the shaded canopy, while the CLM5 did not represent the within-canopy turbulent variation, heat and moisture transfer, and leaf stomatal controls across different canopy layers like that in the CLM-ML model (Bonan

et al., 2021). Although the integrated FAPAR in sunlit and shaded canopies simulated by CLM5 and CLM-ML generally agreed well with each other (Figure S9), the FAPAR varied across the vertical canopy depth in CLM-ML (Figure S10), and the estimated GPP by CLM5 and CLM-ML could be different because of the nonlinear relationship between GPP and FAPAR, since the multi-layer model calculates GPP in each layer and then integrates them over the vertical depth rather than integrates FAPAR first and then calculates GPP based on the integrated total FAPAR. For example, the CLM-ML showed increased FAPAR under lower layers of sunlit–shaded canopy after including CI (Figure S10). CI-induced increase in FAPAR in the lower canopy layers could increase GPP as photosynthesis is most light-limited in such situations (Braghiere et al., 2019) while the CLM5 did not represent the layer varied GPP with layer varied FAPAR. To date, the multi-layer scheme of CLM-ML has not been coupled into the current CLM5 release yet, making it challenging to examine the global impacts if the multi-layer scheme is used and leaving room for future exploration. Novel global remotely sensed vertical canopy profile data such as the observations from NASA's Global Ecosystem Dynamics Investigation (Hancock et al., 2019) may be needed and support such efforts given the considerable vertical heterogeneity of CI, LAI, and biophysical and biogeochemical processes across different layers of canopy (Bonan et al., 2021; Braghiere, Gérard, et al., 2020; Fang, 2021). The vertical canopy structure, the strong angular variations of CI, and the coupling between topographic and CI effects (Hao et al., 2018, 2022), which may also significantly affect estimates of latent/sensible heat, evapotranspiration, and solar-induced chlorophyll fluorescence (Braghiere et al., 2021; Li, Lombardozzi, et al., 2022; Wang et al., 2021), and therefore also need to be further explored.

We showed that the incorporation of CI reduced the discrepancy between the modeled GPP and that of two benchmarking datasets. This indicates the potential importance of CI, although does not imply that CI necessarily improves GPP estimation because we could get the correct answer with wrong reasons due to the uncertainty of the model itself, and the benchmarking datasets (and other global GPP datasets) do not necessarily represent the truth as large uncertainties remain especially in tropical regions (Xie et al., 2020; Zhang & Ye, 2022) as well. Therefore, further comprehensive validation of the benefit of incorporating CI for GPP magnitude, seasonal variation, long-term interannual variations, and even related causal structures (Li, Zhu, et al., 2022; Runge et al., 2019; Yuan, Zhu, Li, et al., 2022; Yuan, Zhu, Riley, et al., 2022; Yuan et al., 2021) is needed when more reliable global GPP and CI data are available at the same spatial scale. In addition, we found that the CI impacts on GPP varied with DRF in CLM5 (Figure S5). However, limited observations are available to constrain global DRF (Chakraborty et al., 2022), and substantial uncertainty in diffuse radiation was identified among different global reanalysis datasets and different directive-diffuse radiation partitioning methods, especially in tropical areas (Chakraborty et al., 2022; Chakraborty & Lee, 2021). The uncertainty of DRF needs to be narrowed and the interactions among atmospheric conditions, canopy structure, and land surface biophysical and biogeochemical processes need further exploration.

5 | CONCLUSIONS

This study explored how CI affects the canopy radiation transfer and photosynthesis rate at a global scale considering the uncertainty from multiple satellite-derived global CI datasets and the seasonal variations of CI. We found significant differences existed among different CI datasets across different biome types, and up to 9%–15% FAPAR of direct radiation and 23%–34% FAPAR of diffuse radiation in sunlit canopy was overestimated and 3%–18% FAPAR of diffuse radiation in shaded canopy was underestimated. CI-induced changes of canopy energy absorption and nitrogen distribution resulted in a significant overestimation of sunlit canopy GPP (5.9–7.2 PgC year^{-1}) and underestimation of shaded GPP (6.9–8.2 PgC year^{-1}) with a net increase in GPP by 1.0 ± 0.12 PgC year^{-1}. The uncertainty of CI products induced GPP variations was larger than that of CI seasonal variations, and up to 50% of GPP interannual variations at tropical regions, which requires further narrowing of the CI uncertainty. Most TBMs do not account for clumping, therefore also have the clumping induced bias in canopy radiation transfer and photosynthesis, and such bias may be amplified by future global greening with increased leaf area and absorbed diffuse radiation. This study highlights the need to reduce CI uncertainty and represent vegetation clumping in TBMs to reduce the systematic bias in past–present–future canopy radiation transfer and photosynthesis simulations.

ORCID

Fa Li https://orcid.org/0000-0002-0625-5587
Dalei Hao https://orcid.org/0000-0001-7154-6332
Qing Zhu https://orcid.org/0000-0003-2441-944X
Kunxiaojia Yuan https://orcid.org/0000-0002-1336-5768
Renato K. Braghiere https://orcid.org/0000-0002-7722-717X
Liming He https://orcid.org/0000-0003-4010-6814
Xiangzhong Luo https://orcid.org/0000-0002-9546-0960
Shanshan Wei https://orcid.org/0000-0002-2831-3864
William J. Riley https://orcid.org/0000-0002-4615-2304
Yelu Zeng https://orcid.org/0000-0003-4267-1841
Min Chen https://orcid.org/0000-0001-6311-7124

REFERENCES

Alton, P., Ellis, R., Los, S., & North, P. (2007). Improved global simulations of gross primary product based on a separate and explicit treatment of diffuse and direct sunlight. *Journal of Geophysical Research: Atmospheres*, 112.

Anav, A., Friedlingstein, P., Beer, C., Ciais, P., Harper, A., Jones, C., Murray-Tortarolo, G., Papale, D., Parazoo, N. C., & Peylin, P. (2015). Spatiotemporal patterns of terrestrial gross primary production: A review. *Reviews of Geophysics*, 53, 785–818.

Baldocchi, D., Ryu, Y., & Keenan, T. (2016). Terrestrial carbon cycle variability. *F1000Research*, 5, 2371.

Baldocchi, D. D., & Wilson, K. B. (2001). Modeling CO₂ and water vapor exchange of a temperate broadleaved forest across hourly to decadal time scales. *Ecological Modelling*, 142, 155–184.

Bodman, R. W., Rayner, P. J., & Karoly, D. J. (2013). Uncertainty in temperature projections reduced using carbon cycle and climate observations. *Nature Climate Change*, 3, 725–729.

Bonan, G. (2019). *Climate change and terrestrial ecosystem modeling*. Cambridge University Press.

Bonan, G. B. (1996). *Land surface model (LSM version 1.0) for ecological, hydrological, and atmospheric studies: Technical description and users guide. Technical note*. National Center for Atmospheric Research.

Bonan, G. B., Levis, S., Kergoat, L., & Oleson, K. W. (2002). Landscapes as patches of plant functional types: An integrating concept for climate and ecosystem models. *Global Biogeochemical Cycles*, 16, 5-1–5-23.

Bonan, G. B., Patton, E. G., Finnigan, J. J., Baldocchi, D. D., & Harman, I. N. (2021). Moving beyond the incorrect but useful paradigm: Reevaluating big-leaf and multilayer plant canopies to model biosphere-atmosphere fluxes – A review. *Agricultural and Forest Meteorology*, 306, 108435.

Braghiere, R. K., Gérard, F., Evers, J. B., Pradal, C., & Pagès, L. (2020). Simulating the effects of water limitation on plant biomass using a

3D functional–structural plant model of shoot and root driven by soil hydraulics. *Annals of Botany*, 126, 713–728.

Braghiere, R. K., Quaife, T., Black, E., He, L., & Chen, J. (2019). Underestimation of global photosynthesis in earth system models due to representation of vegetation structure. *Global Biogeochemical Cycles*, 33, 1358–1369.

Braghiere, R. K., Quaife, T., Black, E., Ryu, Y., Chen, Q., De Kauwe, M. G., & Baldocchi, D. (2020). Influence of sun zenith angle on canopy clumping and the resulting impacts on photosynthesis. *Agricultural and Forest Meteorology*, 291, 108065.

Braghiere, R. K., Wang, Y., Doughty, R., Sousa, D., Magney, T., Widlowski, J.-L., Longo, M., Bloom, A. A., Worden, J., & Gentine, P. (2021). Accounting for canopy structure improves hyperspectral radiative transfer and sun-induced chlorophyll fluorescence representations in a new generation earth system model. *Remote Sensing of Environment*, 261, 112497.

Braghiere, R. K., Yamasoe, M. A., Évora do Rosário, N. M., Ribeiro da Rocha, H., de Souza Nogueira, J., & de Araújo, A. C. (2020). Characterization of the radiative impact of aerosols on CO_2 and energy fluxes in the Amazon deforestation arch using artificial neural networks. *Atmospheric Chemistry and Physics*, 20, 3439–3458.

Chakraborty, T., & Lee, X. (2021). Large differences in diffuse solar radiation among current-generation reanalysis and satellite-derived products. *Journal of Climate*, 34, 6635–6650.

Chakraborty, T., Lee, X., & Lawrence, D. (2022). Diffuse radiation forcing constraints on gross primary productivity and global terrestrial evapotranspiration. *Earth's Future*, 10, e2022EF002805.

Chen, B., Liu, J., Chen, J. M., Croft, H., Gonsamo, A., He, L., & Luo, X. (2016). Assessment of foliage clumping effects on evapotranspiration estimates in forested ecosystems. *Agricultural and Forest Meteorology*, 216, 82–92.

Chen, B., Lu, X., Wang, S., Chen, J. M., Liu, Y., Fang, H., Liu, Z., Jiang, F., Arain, M. A., & Chen, J. (2021). Evaluation of clumping effects on the estimation of global terrestrial evapotranspiration. *Remote Sensing*, 13, 4075.

Chen, J., Liu, J., Cihlar, J., & Goulden, M. (1999). Daily canopy photosynthesis model through temporal and spatial scaling for remote sensing applications. *Ecological Modelling*, 124, 99–119.

Chen, J., Menges, C., & Leblanc, S. (2005). Global mapping of foliage clumping index using multi-angular satellite data. *Remote Sensing of Environment*, 97, 447–457.

Chen, J. M., & Black, T. (1992). Defining leaf area index for non-flat leaves. *Plant, Cell & Environment*, 15, 421–429.

Chen, J. M., Mo, G., Pisek, J., Liu, J., Deng, F., Ishizawa, M., & Chan, D. (2012). Effects of foliage clumping on the estimation of global terrestrial gross primary productivity. *Global Biogeochemical Cycles*, 26.

Chen, M., & Zhuang, Q. (2014). Evaluating aerosol direct radiative effects on global terrestrial ecosystem carbon dynamics from 2003 to 2010. *Tellus B: Chemical and Physical Meteorology*, 66, 21808.

Clark, D., Mercado, L., Sitch, S., Jones, C., Gedney, N., Best, M., Pryor, M., Rooney, G., Essery, R., & Blyth, E. (2011). The joint UK land environment simulator (JULES), model description – Part 2: Carbon fluxes and vegetation dynamics. *Geoscientific Model Development*, 4, 701–722.

Collins, M., Knutti, R., Arblaster, J., Dufresne, J.-L., Fichefet, T., Friedlingstein, P., Gao, X., Gutowski, W. J., Johns, T., & Krinner, G. (2013). Long-term climate change: Projections, commitments and irreversibility. In *Climate change 2013 – The physical science basis: Contribution of working group I to the fifth assessment report of the Intergovernmental Panel on Climate Change* (pp. 1029–1136). Cambridge University Press.

De Pury, D., & Farquhar, G. (1997). Simple scaling of photosynthesis from leaves to canopies without the errors of big-leaf models. *Plant, Cell & Environment*, 20, 537–557.

Dickinson, R. E. (1983). Land surface processes and climate—Surface albedos and energy balance. In *Advances in geophysics* (pp. 305–353). Elsevier.

Dirmeyer, P. A., Gao, X., Zhao, M., Guo, Z., Oki, T., & Hanasaki, N. (2006). GSWP-2: Multimodel analysis and implications for our perception of the land surface. *Bulletin of the American Meteorological Society*, 87, 1381–1398.

Durand, M., Murchie, E. H., Lindfors, A. V., Urban, O., Aphalo, P. J., & Robson, T. M. (2021). Diffuse solar radiation and canopy photosynthesis in a changing environment. *Agricultural and Forest Meteorology*, 311, 108684.

Eyring, V., Bony, S., Meehl, G. A., Senior, C. A., Stevens, B., Stouffer, R. J., & Taylor, K. E. (2016). Overview of the coupled model Intercomparison project phase 6 (CMIP6) experimental design and organization. *Geoscientific Model Development*, 9, 1937–1958.

Fang, H. (2021). Canopy clumping index (CI): A review of methods, characteristics, and applications. *Agricultural and Forest Meteorology*, 303, 108374.

Friedl, M., & Sulla-Menashe, D. (2015). MCD12Q1 MODIS/Terra+ aqua land cover type yearly L3 global 500m SIN grid V006 [data set]. *NASA EOSDIS Land Processes DAAC*, 10, 200.

Golaz, J. C., Caldwell, P. M., Van Roekel, L. P., Petersen, M. R., Tang, Q., Wolfe, J. D., Abeshu, G., Anantharaj, V., Asay-Davis, X. S., & Bader, D. C. (2019). The DOE E3SM coupled model version 1: Overview and evaluation at standard resolution. *Journal of Advances in Modeling Earth Systems*, 11, 2089–2129.

Gorelick, N., Hancher, M., Dixon, M., Ilyushchenko, S., Thau, D., & Moore, R. (2017). Google earth engine: Planetary-scale geospatial analysis for everyone. *Remote Sensing of Environment*, 202, 18–27.

Goudriaan, J. (1977). *Crop micrometeorology: A simulation study.* Wageningen University and Research.

Gu, L., Fuentes, J. D., Shugart, H. H., Staebler, R. M., & Black, T. A. (1999). Responses of net ecosystem exchanges of carbon dioxide to changes in cloudiness: Results from two North American deciduous forests. *Journal of Geophysical Research: Atmospheres*, 104, 31421–31434.

Hancock, S., Armston, J., Hofton, M., Sun, X., Tang, H., Duncanson, L. I., Kellner, J. R., & Dubayah, R. (2019). The GEDI simulator: A large-footprint waveform lidar simulator for calibration and validation of spaceborne missions. *Earth and Space Science*, 6, 294–310.

Hao, D., Bisht, G., Huang, M., Ma, P. L., Tesfa, T., Lee, W. L., Gu, Y., & Leung, L. R. (2022). Impacts of sub-grid topographic representations on surface energy balance and boundary conditions in the E3SM Land Model: A case study in Sierra Nevada. *Journal of Advances in Modeling Earth Systems*, 14, e2021MS002862.

Hao, D., Wen, J., Xiao, Q., Wu, S., Lin, X., You, D., & Tang, Y. (2018). Modeling anisotropic reflectance over composite sloping terrain. *IEEE Transactions on Geoscience and Remote Sensing*, 56, 3903–3923.

He, L., Chen, J. M., Gonsamo, A., Luo, X., Wang, R., Liu, Y., & Liu, R. (2018). Changes in the shadow: The shifting role of shaded leaves in global carbon and water cycles under climate change. *Geophysical Research Letters*, 45, 5052–5061.

He, L., Chen, J. M., Pisek, J., Schaaf, C. B., & Strahler, A. H. (2012). Global clumping index map derived from the MODIS BRDF product. *Remote Sensing of Environment*, 119, 118–130.

He, L., Liu, J., Chen, J. M., Croft, H., Wang, R., Sprintsin, M., Zheng, T., Ryu, Y., Pisek, J., & Gonsamo, A. (2016). Inter-and intra-annual variations of clumping index derived from the MODIS BRDF product. *International Journal of Applied Earth Observation and Geoinformation*, 44, 53–60.

Hijmans, R. J., Cameron, S. E., Parra, J. L., Jones, P. G., & Jarvis, A. (2005). Very high resolution interpolated climate surfaces for global land areas. *International Journal of Climatology: A Journal of the Royal Meteorological Society*, 25, 1965–1978.

Hoffmann, P., Reinhart, V., Rechid, D., de Noblet-Ducoudré, N., Davin, E. L., Asmus, C., Bechtel, B., Böhner, J., Katragkou, E., & Luyssaert, S. (2021). High-resolution land-use land-cover change data for regional climate modelling applications over Europe – Part 2: Historical and future changes. *Earth System Science Data Discussions*, 1–43.

Jian, J., Bailey, V., Dorheim, K., Konings, A. G., Hao, D., Shiklomanov, A. N., Snyder, A., Steele, M., Teramoto, M., & Vargas, R. (2022).

Historically inconsistent productivity and respiration fluxes in the global terrestrial carbon cycle. *Nature Communications*, 13, 1–9.

Jiao, Z., Dong, Y., Schaaf, C. B., Chen, J. M., Román, M., Wang, Z., Zhang, H., Ding, A., Erb, A., & Hill, M. J. (2018). An algorithm for the retrieval of the clumping index (CI) from the MODIS BRDF product using an adjusted version of the kernel-driven BRDF model. *Remote Sensing of Environment*, 209, 594–611.

Jung, M., Reichstein, M., & Bondeau, A. (2009). Towards global empirical upscaling of FLUXNET eddy covariance observations: Validation of a model tree ensemble approach using a biosphere model. *Biogeosciences*, 6, 2001–2013.

Jung, M., Reichstein, M., Margolis, H. A., Cescatti, A., Richardson, A. D., Arain, M. A., Arneth, A., Bernhofer, C., Bonal, D., & Chen, J. (2011). Global patterns of land-atmosphere fluxes of carbon dioxide, latent heat, and sensible heat derived from eddy covariance, satellite, and meteorological observations. *Journal of Geophysical Research: Biogeosciences*, 116.

Jung, M., Reichstein, M., Schwalm, C. R., Huntingford, C., Sitch, S., Ahlström, A., Arneth, A., Camps-Valls, G., Ciais, P., & Friedlingstein, P. (2017). Compensatory water effects link yearly global land CO_2 sink changes to temperature. *Nature*, 541, 516–520.

Knohl, A., & Baldocchi, D. D. (2008). Effects of diffuse radiation on canopy gas exchange processes in a forest ecosystem. *Journal of Geophysical Research: Biogeosciences*, 113.

Knyazikhin, Y. (1999). *MODIS leaf area index (LAI) and fraction of photosynthetically active radiation absorbed by vegetation (FPAR) product (MOD 15) algorithm theoretical basis document*. http://eospso.gsfc.nasa.gov/atbd/modistabls.heml

Knyazikhin, Y., Martonchik, J., Myneni, R. B., Diner, D., & Running, S. W. (1998). Synergistic algorithm for estimating vegetation canopy leaf area index and fraction of absorbed photosynthetically active radiation from MODIS and MISR data. *Journal of Geophysical Research: Atmospheres*, 103, 32257–32275.

Krinner, G., Viovy, N., de Noblet-Ducoudré, N., Ogée, J., Polcher, J., Friedlingstein, P., Ciais, P., Sitch, S., & Prentice, I. C. (2005). A dynamic global vegetation model for studies of the coupled atmosphere-biosphere system. *Global Biogeochemical Cycles*, 19.

Law, B. E., Cescatti, A., & Baldocchi, D. D. (2001). Leaf area distribution and radiative transfer in open-canopy forests: Implications for mass and energy exchange. *Tree Physiology*, 21, 777–787.

Lawrence, D. M., Fisher, R. A., Koven, C. D., Oleson, K. W., Swenson, S. C., Bonan, G., Collier, N., Ghimire, B., van Kampenhout, L., & Kennedy, D. (2019). The community land model version 5: Description of new features, benchmarking, and impact of forcing uncertainty. *Journal of Advances in Modeling Earth Systems*, 11, 4245–4287.

Lawrence, P. J., & Chase, T. N. (2007). Representing a new MODIS consistent land surface in the community land model (CLM 3.0). *Journal of Geophysical Research: Biogeosciences*, 112, G1.

Le Quéré, C., Andrew, R. M., Friedlingstein, P., Sitch, S., Hauck, J., Pongratz, J., Pickers, P. A., Korsbakken, J. I., Peters, G. P., & Canadell, J. G. (2018). Global carbon budget 2018. *Earth System Science Data*, 10, 2141–2194.

Leblanc, S. G., Chen, J. M., White, H. P., Latifovic, R., Lacaze, R., & Roujean, J.-L. (2005). Canada-wide foliage clumping index mapping from multiangular POLDER measurements. *Canadian Journal of Remote Sensing*, 31, 364–376.

Li, F., Hao, D., Zhu, Q., Yuan, K., Braghiere, R. K., He, L., Luo, X., Wei, S., Riley, W. J., Zeng, Y., & Chen, M. (2022). Vegetation clumping modulates global photosynthesis through adjusting canopy light environment. *Global Change Biology*. https://doi.org/10.1111/gcb.16503

Li, F., Zhu, Q., Riley, W. J., Yuan, K., Wu, H., & Gui, Z. (2022). Wetter California projected by CMIP6 models with observational constraints under a high GHG emission scenario. *Earth's Futures*, 10, e2022EF002694.

Li, R., Lombardozzi, D., Shi, M., Frankenberg, C., Parazoo, N. C., Köhler, P., Yi, K., Guan, K., & Yang, X. (2022). Representation of leaf-to-canopy radiative transfer processes improves simulation of far-red solar-induced chlorophyll fluorescence in the community land model version 5. *Journal of Advances in Modeling Earth Systems*, 14, e2021MS002747.

Li, X., & Xiao, J. (2019). Mapping photosynthesis solely from solar-induced chlorophyll fluorescence: A global, fine-resolution dataset of gross primary production derived from OCO-2. *Remote Sensing*, 11, 2563.

Li, X., Xiao, J., He, B., Altaf Arain, M., Beringer, J., Desai, A. R., Emmel, C., Hollinger, D. Y., Krasnova, A., & Mammarella, I. (2018). Solar-induced chlorophyll fluorescence is strongly correlated with terrestrial photosynthesis for a wide variety of biomes: First global analysis based on OCO-2 and flux tower observations. *Global Change Biology*, 24, 3990–4008.

Loew, A., Van Bodegom, P., Widlowski, J.-L., Otto, J., Quaife, T., Pinty, B., & Raddatz, T. (2014). Do we (need to) care about canopy radiation schemes in DGVMs? Caveats and potential impacts. *Biogeosciences*, 11, 1873–1897.

Luo, X., Chen, J. M., Liu, J., Black, T. A., Croft, H., Staebler, R., He, L., Arain, M. A., Chen, B., & Mo, G. (2018). Comparison of big-leaf, two-big-leaf, and two-leaf upscaling schemes for evapotranspiration estimation using coupled carbon-water modeling. *Journal of Geophysical Research: Biogeosciences*, 123, 207–225.

Luo, X., Croft, H., Chen, J. M., He, L., & Keenan, T. F. (2019). Improved estimates of global terrestrial photosynthesis using information on leaf chlorophyll content. *Global Change Biology*, 25, 2499–2514.

Martín Belda, D., Anthoni, P., Wårlind, D., Olin, S., Schurgers, G., Tang, J., Smith, B., & Arneth, A. (2022). LPJ-GUESS/LSMv1. 0: a next-generation land surface model with high ecological realism. *Geoscientific Model Development*, 15(17), 6709–6745.

Medlyn, B. E., Duursma, R. A., Eamus, D., Ellsworth, D. S., Prentice, I. C., Barton, C. V., Crous, K. Y., De Angelis, P., Freeman, M., & Wingate, L. (2011). Reconciling the optimal and empirical approaches to modelling stomatal conductance. *Global Change Biology*, 17, 2134–2144.

Mercado, L. M., Bellouin, N., Sitch, S., Boucher, O., Huntingford, C., Wild, M., & Cox, P. M. (2009). Impact of changes in diffuse radiation on the global land carbon sink. *Nature*, 458, 1014–1017.

Mohammed, G. H., Colombo, R., Middleton, E. M., Rascher, U., van der Tol, C., Nedbal, L., Goulas, Y., Pérez-Priego, O., Damm, A., & Meroni, M. (2019). Remote sensing of solar-induced chlorophyll fluorescence (SIF) in vegetation: 50 years of progress. *Remote Sensing of Environment*, 231, 111177.

Myneni, R. B., Hoffman, S., Knyazikhin, Y., Privette, J., Glassy, J., Tian, Y., Wang, Y., Song, X., Zhang, Y., & Smith, G. (2002). Global products of vegetation leaf area and fraction absorbed PAR from year one of MODIS data. *Remote Sensing of Environment*, 83, 214–231.

Nilson, T. (1971). A theoretical analysis of the frequency of gaps in plant stands. *Agricultural Meteorology*, 8, 25–38.

Norman, J. M. (1993). Scaling processed between leaf and canopy levels. In J. Ehlringer & C. B. Field (Eds.), *Scaling physiological processes: Leaf to globe* (pp. 41–76). Academic Press.

Norman, J. M., & Welles, J. M. (1983). Radiative transfer in an array of canopies 1. *Agronomy Journal*, 75(3), 481–488.

Piao, S., Ciais, P., Friedlingstein, P., de Noblet-Ducoudré, N., Cadule, P., Viovy, N., & Wang, T. (2009). Spatiotemporal patterns of terrestrial carbon cycle during the 20th century. *Global Biogeochemical Cycles*, 23.

Piao, S., Friedlingstein, P., Ciais, P., Zhou, L., & Chen, A. (2006). Effect of climate and CO_2 changes on the greening of the Northern Hemisphere over the past two decades. *Geophysical Research Letters*, 33.

Piao, S., Sitch, S., Ciais, P., Friedlingstein, P., Peylin, P., Wang, X., Ahlström, A., Anav, A., Canadell, J. G., & Cong, N. (2013). Evaluation of terrestrial carbon cycle models for their response to climate variability and to CO_2 trends. *Global Change Biology*, 19, 2117–2132.

Piao, S., Wang, X., Park, T., Chen, C., Lian, X., He, Y., Bjerke, J. W., Chen, A., Ciais, P., & Tømmervik, H. (2020). Characteristics, drivers and feedbacks of global greening. *Nature Reviews Earth & Environment*, 1, 14–27.

Pisek, J., Chen, J. M., & Nilson, T. (2011). Estimation of vegetation clumping index using MODIS BRDF data. *International Journal of Remote Sensing*, 32, 2645–2657.

Ross, J. (1981). *The radiation regime and architecture of plant stands.* Springer Science & Business Media.

Runge, J., Bathiany, S., Bollt, E., Camps-Valls, G., Coumou, D., Deyle, E., Glymour, C., Kretschmer, M., Mahecha, M. D., & Muñoz-Marí, J. (2019). Inferring causation from time series in earth system sciences. *Nature Communications*, 10, 1–13.

Running, S. W., Nemani, R. R., Heinsch, F. A., Zhao, M., Reeves, M., & Hashimoto, H. (2004). A continuous satellite-derived measure of global terrestrial primary production. *Bioscience*, 54, 547–560.

Ryu, Y., Baldocchi, D. D., Kobayashi, H., Van Ingen, C., Li, J., Black, T. A., Beringer, J., Van Gorsel, E., Knohl, A., & Law, B. E. (2011). Integration of MODIS land and atmosphere products with a coupled-process model to estimate gross primary productivity and evapotranspiration from 1 km to global scales. *Global Biogeochemical Cycles*, 25.

Ryu, Y., Berry, J. A., & Baldocchi, D. D. (2019). What is global photosynthesis? History, uncertainties and opportunities. *Remote Sensing of Environment*, 223, 95–114.

Ryu, Y., Nilson, T., Kobayashi, H., Sonnentag, O., Law, B. E., & Baldocchi, D. D. (2010). On the correct estimation of effective leaf area index: Does it reveal information on clumping effects? *Agricultural and Forest Meteorology*, 150, 463–472.

Schlund, M., Eyring, V., Camps-Valls, G., Friedlingstein, P., Gentine, P., & Reichstein, M. (2020). Constraining uncertainty in projected gross primary production with machine learning. *Journal of Geophysical Research: Biogeosciences*, 125, e2019JG005619.

Sellers, P. J. (1985). Canopy reflectance, photosynthesis and transpiration. *International Journal of Remote Sensing*, 6, 1335–1372.

Smith, B., Prentice, I. C., & Sykes, M. T. (2001). Representation of vegetation dynamics in the modelling of terrestrial ecosystems: Comparing two contrasting approaches within European climate space. *Global Ecology and Biogeography*, 10, 621–637.

Still, C., Riley, W., Biraud, S., Noone, D., Buenning, N., Randerson, J., Torn, M., Welker, J., White, J., & Vachon, R. (2009). Influence of clouds and diffuse radiation on ecosystem-atmosphere CO_2 and $CO^{18}O$ exchanges. *Journal of Geophysical Research: Biogeosciences*, 114.

Tramontana, G., Jung, M., Schwalm, C. R., Ichii, K., Camps-Valls, G., Ráduly, B., Reichstein, M., Arain, M. A., Cescatti, A., & Kiely, G. (2016). Predicting carbon dioxide and energy fluxes across global FLUXNET sites with regression algorithms. *Biogeosciences*, 13, 4291–4313.

Verhoef, A., & Egea, G. (2014). Modeling plant transpiration under limited soil water: Comparison of different plant and soil hydraulic parameterizations and preliminary implications for their use in land surface models. *Agricultural and Forest Meteorology*, 191, 22–32.

Walcroft, A. S., Brown, K. J., Schuster, W. S., Tissue, D. T., Turnbull, M. H., Griffin, K. L., & Whitehead, D. (2005). Radiative transfer and carbon assimilation in relation to canopy architecture, foliage area distribution and clumping in a mature temperate rainforest canopy in New Zealand. *Agricultural and Forest Meteorology*, 135, 326–339.

Wang, X., Wu, J., Chen, M., Xu, X., Wang, Z., Wang, B., Wang, C., Piao, S., Lin, W., & Miao, G. (2018). Field evidences for the positive effects of aerosols on tree growth. *Global Change Biology*, 24, 4983–4992.

Wang, Y., Köhler, P., He, L., Doughty, R., Braghiere, R. K., Wood, J. D., & Frankenberg, C. (2021). Testing stomatal models at the stand level in deciduous angiosperm and evergreen gymnosperm forests using CliMA Land (v0.1). *Geoscientific Model Development*, 14, 6741–6763.

Wang, Y., & Polglase, P. (1995). Carbon balance in the tundra, boreal forest and humid tropical forest during climate change: Scaling up from leaf physiology and soil carbon dynamics. *Plant, Cell & Environment*, 18, 1226–1244.

Wang, Y.-P., & Leuning, R. (1998). A two-leaf model for canopy conductance, photosynthesis and partitioning of available energy I: Model description and comparison with a multi-layered model. *Agricultural and Forest Meteorology*, 91, 89–111.

Wang, Z., Schaaf, C. B., Sun, Q., Shuai, Y., & Román, M. O. (2018). Capturing rapid land surface dynamics with collection V006 MODIS BRDF/NBAR/albedo (MCD43) products. *Remote Sensing of Environment*, 207, 50–64.

Wei, S., & Fang, H. (2016). Estimation of canopy clumping index from MISR and MODIS sensors using the normalized difference hotspot and darkspot (NDHD) method: The influence of BRDF models and solar zenith angle. *Remote Sensing of Environment*, 187, 476–491.

Wei, S., Fang, H., Schaaf, C. B., He, L., & Chen, J. M. (2019). Global 500 m clumping index product derived from MODIS BRDF data (2001–2017). *Remote Sensing of Environment*, 232, 111296.

Williams, I. N., Riley, W. J., Kueppers, L. M., Biraud, S. C., & Torn, M. S. (2016). Separating the effects of phenology and diffuse radiation on gross primary productivity in winter wheat. *Journal of Geophysical Research: Biogeosciences*, 121, 1903–1915.

Xie, X., Li, A., Tan, J., Lei, G., Jin, H., & Zhang, Z. (2020). Uncertainty analysis of multiple global GPP datasets in characterizing the lagged effect of drought on photosynthesis. *Ecological Indicators*, 113, 106224.

Yan, H., Wang, S. Q., Huete, A., & Shugart, H. H. (2019). Effects of light component and water stress on photosynthesis of Amazon rainforests during the 2015/2016 El Niño drought. *Journal of Geophysical Research: Biogeosciences*, 124, 1574–1590.

Yan, K., Park, T., Yan, G., Liu, Z., Yang, B., Chen, C., Nemani, R. R., Knyazikhin, Y., & Myneni, R. B. (2016). Evaluation of MODIS LAI/FPAR product collection 6. Part 2: Validation and intercomparison. *Remote Sensing*, 8, 460.

Yuan, K., Zhu, Q., Li, F., Riley, W. J., Torn, M., Chu, H., McNicol, G., Chen, M., Knox, S., & Delwiche, K. (2022). Causality guided machine learning model on wetland CH_4 emissions across global wetlands. *Agricultural and Forest Meteorology*, 324, 109115.

Yuan, K., Zhu, Q., Riley, W. J., Li, F., & Wu, H. (2022). Understanding and reducing the uncertainties of land surface energy flux partitioning within CMIP6 land models. *Agricultural and Forest Meteorology*, 319, 108920.

Yuan, K., Zhu, Q., Zheng, S., Zhao, L., Chen, M., Riley, W. J., Cai, X., Ma, H., Li, F., Wu, H., & Chen, L. (2021). Deforestation reshapes land-surface energy-flux partitioning. *Environmental Research Letters*, 16(2), 024014. https://doi.org/10.1088/1748-9326/abd8f9

Zhang, Y., Guanter, L., Berry, J. A., Joiner, J., van der Tol, C., Huete, A., Gitelson, A., Voigt, M., & Köhler, P. (2014). Estimation of vegetation photosynthetic capacity from space-based measurements of chlorophyll fluorescence for terrestrial biosphere models. *Global Change Biology*, 20, 3727–3742.

Zhang, Y., & Ye, A. (2022). Improving global gross primary productivity estimation by fusing multi-source data products. *Heliyon*, 8, e09153.

Zhao, M., Running, S. W., & Nemani, R. R. (2006). Sensitivity of moderate resolution imaging spectroradiometer (MODIS) terrestrial primary production to the accuracy of meteorological reanalyses. *Journal of Geophysical Research: Biogeosciences*, 111.

SUPPORTING INFORMATION

Additional supporting information can be found online in the Supporting Information section at the end of this article.